Effect of Cooling Rate on Dopant Spatial Localization and Phase Transformation in Cu-Doped Y-Stabilized ZrO$_2$ Nanopowders

Nadiia Korsunska, Mykola Baran, Igor Vorona, Valentyna Nosenko, Serhiy Lavoryk, Yuliya Polishchuk, Vasyl Kladko, Xavier Portier, and Larysa Khomenkova*

The effect of calcination temperature ($T_C = 500$–$1000\,^\circ$C) and cooling rate on the dopant distribution in Cu-doped Y-stabilized ZrO$_2$ nanopowders is studied. The powders are produced by co-precipitation technique and investigated by attenuated total reflection, UV-vis diffuse reflectance, electron paramagnetic resonance, and transmission electron microscopy methods. The cooling rate is found to affect the amount of Cu substances on grain surface, the powders subjected to fast cooling (quenching) showed higher amount of Cu-related complexes on the grains' surface than their counterparts cooled with furnace after calcination. It is observed that Cu impurities diffuse inside ZrO$_2$ grains from Cu-related surface substances when $T_C < 800\,^\circ$C. This process is accompanied by the enhancement of 275-nm absorption band caused by oxygen vacancies formation. For $T_C > 800\,^\circ$C, outward migration of Cu dopants takes place. Simultaneously, the intensity of 275-nm absorption band decreases, the monoclinic ZrO$_2$ phase forms and its contribution rises with T_C. It is proposed that monoclinic phase formation is caused by the replacement of Cu atoms from lattice sites to interstitials leading to an appearance of the channels for Y out-diffusion via cation vacancies and destabilization of ZrO$_2$ tetragonal phase.

1. Introduction

Zirconia has unique properties as catalysts and supports mainly because of high surface area, the preservation of both acid and basic sites and possession of redox properties.[1,2] Being mechanically and thermally stable, ZrO$_2$ is used as structural supports in many catalytic applications.[1–11]

In recent years, Cu-doped ZrO$_2$ powders are intensively developed as catalysts because the modification of ZrO$_2$ with Cu (or CuO) significantly improves the catalytic activity and selectivity in methanol,[3,4] NO or N$_2$O decomposition, CO and CO$_2$ hydrogenation.[5–7]

The ZrO$_2$ phases, i.e., monoclinic (*m*), tetragonal (*t*), or cubic (*c*), influence the catalytic performance.[6] The effect of Cu dopant on the structural characteristics of the Cu-ZrO$_2$ composites, as well as their catalytic properties, was extensively studied for *m*-ZrO$_2$ powders.[8,9] It was shown in Ref. [10] that CuO/*m*-ZrO$_2$ catalysts are more active in methanol synthesis than CuO/*t*-ZrO$_2$. However, it was also reported in Refs. [4,7] that *t*-ZrO$_2$ phase exhibits better catalytic properties than m-ZrO$_2$. Such behavior can be caused by the difference in the preparation techniques used for doped powders production.

Most experiments were performed on Cu-ZrO$_2$ powders produced by impregnation method that led to predominant localization of copper on the surface of ZrO$_2$ crystallites or in their near-surface region. At the same time, co-precipitation technique allows obtaining the powders which contain the dopants both inside crystallite volume and at their surface, simultaneously.[4,11,12] It was shown that their catalytic properties depend significantly on doping level and Cu spatial localization.

It is known that for stabilization of *t*-ZrO$_2$ phase, the doping with yttrium is often used. However, in comparison with Cu-ZrO$_2$, the structural properties of (Cu,Y)-codoped ZrO$_2$ and the spatial distribution of the impurities can differ. For instance, in Ref. [13] it was shown that Cu addition to Y-stabilized ZrO$_2$ lowers the temperature of *t-m* phase transformation and favors

Prof. N. Korsunska, Dr. M. Baran, Dr. I. Vorona, Dr. V. Nosenko, Dr. S. Lavoryk, Y. Polishchuk, Prof. V. Kladko, Dr. L. Khomenkova
V. Lashkaryov Institute of Semiconductor Physics of National Academy of Sciences of Ukraine
45 pr. Nauky, 03028 Kyiv, Ukraine
E-mail: khomen@ukr.net

Dr. S. Lavoryk
NanoMedTech LLC
68 Antonovycha Str., 03680 Kyiv, Ukraine

Prof. X. Portier
CIMAP Normandie Univ, ENSICAEN, UNICAEN, CEA, CNRS
6 Boulevard Maréchal Juin, 14050 Caen, France

The ORCID identification number(s) for the author(s) of this article can be found under https://doi.org/10.1002/pssc.201700183.

**ADVANCED
SCIENCE NEWS**

www.advancedsciencenews.com

pss
physica status solidi c

www.pss-c.com

the formation of Y cuprate on ZrO_2 crystallite surface at elevated temperatures. It was also demonstrated for the powders produced by co-precipitation approach that structural properties of (Cu,Y)-codoped ZrO_2 powders depends not only on Cu content, but also on calcination temperature. It was shown that the calcination of the powders at 500–700 °C caused the enrichment in copper of the volume of ZrO_2 nanocrystals due to Cu in-diffusion from surface complexes. The increasing of calcination temperature from 800 up to 1000 °C resulted in outward Cu diffusion, t-m structural ZrO_2 transformation and appearance of dispersed and crystalline CuO on crystallites surface.

It is worth to point out that, to our knowledge, the effect of the cooling rate on the structural properties and dopant distribution in (Cu,Y)-codoped powders was rarely addressed.[12,14] Meanwhile, the cooling rate can affect significantly the spatial distribution of dopants. In present work, optical and structural properties of (Cu,Y)-codoped ZrO_2 powders were studied versus cooling rate in order to find the ways to control surface/volume spatial Cu localization.

2. Experimental Section

Cu-doped Y-stabilized ZrO_2 nanopowders were synthesized by a co-precipitation technique. Zr, Y, and Cu nitrates were mixed in molar ratio of $ZrO(NO_3)_2$:$Y(NO_3)_3$:$Cu(NO_3)_2 = 89$:3:8 in distilled water. With such a composition the Y_2O_3 and CuO content of 3 and 8 mol.% were obtained, respectively. For chemical precipitation, the 6 wt.% ammonia solution was used with pH = 10–11. The precipitates were washed to pH = 7 with distilled water and filtered. The microwave irradiation (700 W, 2.45 GHz) was used to dry the precipitates. Then, xerogels were calcinated at $T = 500$–1100 °C for 2 h. Afterwards, they were either slowly (during 2 h) cooled with the furnace to room temperature (S-set) or quenched (during few seconds) by their fast removing from the furnace (R-set). The optical and structural properties of the powders were studied by attenuated total reflection, UV-visible diffuse reflectance, electron paramagnetic resonance, X-ray diffraction, and transmission electron microscopy methods. More details about experimental procedure can be found in Refs. [12,15].

3. Results and Discussion

3.1. TEM Observations

TEM observations were performed for both sets of powders, and hereafter, the results demonstrated pronounced variations of the crystalline structure. As one can see from **Figure 1**(a and b) xerogel has an amorphous structure. Calcination of the initial xerogel at different temperatures results in the formation of nanocrystals. These latter were found to be well dispersed and had a mean size of about ≈14 nm ($T_C = 600$ °C). Calcination at higher temperatures results in the nanocrystals growing (Figure 1c–h). Their mean size increases up to ≈46 nm ($T_C = 900$ °C). It is worth to point out that annealing during $t > 2$ h results in grain growing. For instance, for $T = 900$ °C and
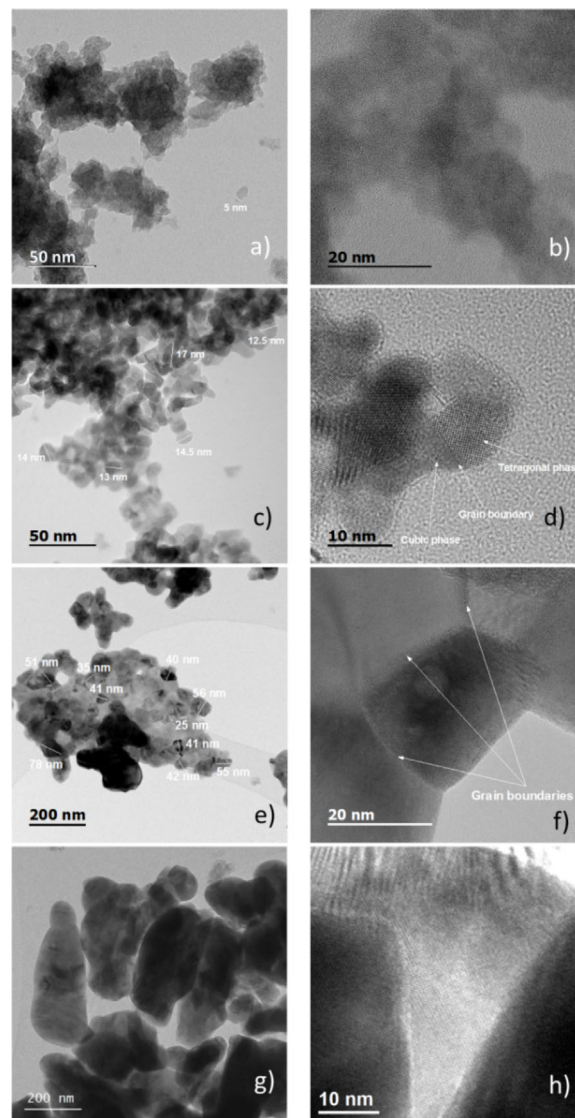

Figure 1. High-resolution TEM images of initial xerogel (a and b) and the powders calcinated at 600 (c and d) and 900 °C (e–h) followed by slow cooling (e and f) and quenching (g and h).

$t = 3$ h, the mean grain size was found to be ≈70 nm (Figure 1g and h). However, the longer time results in the saturation of the grain sizes without transformation of their crystalline structure as demonstrated in Ref. [15]. When $T = 1000$–1100 °C, the mean size increases further, but it shows also a saturation. For the powders calcinated at 1000 and 1100 °C, it was about 70 nm for monoclinic grains and about 35 nm for tetragonal grains.

It was observed that the cooling rate did not affect significantly the nanocrystal sizes whatever the calcination temperature, but it controls the type of crystalline structure. In fact, for the powders calcinated at $T = 600$ °C, the nanocrystals were found to be with tetragonal and cubic structures (Figure 1c and d), while for $T = 900$ °C, the main part of nanocrystals was of monoclinic phase (Figure 1e and f). Besides, large particles were found to be

composed of smaller nanocrystals with grain boundaries (Figure 1e–h). The presence of tetragonal and cubic grains in the powders calcinated at 900 °C was also detected, but their amount was much lower.

These TEM results are consistent with our earlier study of Y-doped ZrO_2 powders.[16,17] It was observed that the increase of the calcination time resulted in the growing of the nanocrystal sizes while their structure was mostly unchanged. These results are also in an agreement with the data of Refs. [12,15] in which these powders were studied by X-ray diffraction method. To get insight on the effect of calcination temperature and cooling rate on the optical properties of the powders, the same samples were studied by infrared attenuated total reflectance (ATR) and UV-vis diffuse reflectance.

3.2. Infrared Absorption Spectra

The ATR spectra of both sets of samples are shown in **Figure 2**. The spectra of all powders demonstrate Zr-O related vibration bands in the range of 500–850 cm^{-1}. Besides, the powders calcinated at $T_c \leq 800$ °C whatever the cooling rate and those calcinated at 1100 °C followed by quenching showed vibration
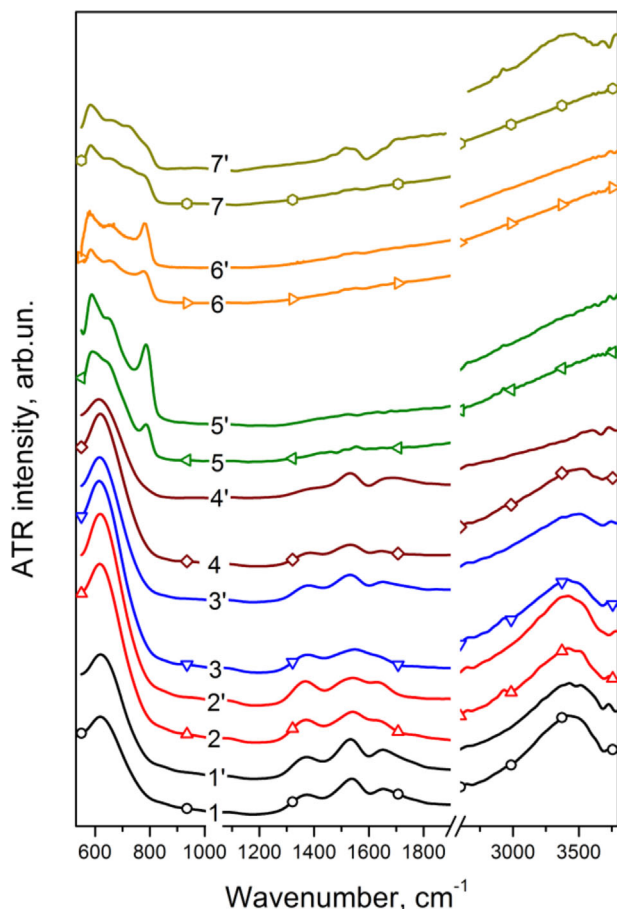

Figure 2. ATR spectra of the powders calcinated at $T_C = 500$ (1, 1'), 600 (2, 2'), 700 (3, 3'), 800 (4, 4'), 900 (5, 5'), 1000 (6, 6'), and 1100 °C (7, 7') followed by slow cooling (1–7) and quenching (1'–7').

bands in the range of 1300–1700 and 3000–3700 cm^{-1} corresponding to vibrations of water molecules and/or OH-groups.

The spectra of the powders of S- and R-sets calcinated at $T_c \leq 800$ °C were found to be similar. They demonstrate a broad band at ≈ 615–625 cm^{-1} that is attributed to absorption band of ZrO_2 lattice in tetragonal and/or cubic phase.[12,18] When T_C increases up to 900 °C, the bands peaked at ≈ 575 and ≈ 770 cm^{-1} appeared indicating the presence of monoclinic phase.[12] However, for the samples of R-set, its signature is more pronounced (Figure 2, curves 5, 5', 6, 6'). This finding agrees with XRD results showed appearance of monoclinic phase with contribution being less than 3% even at $T_C = 800$ °C.[15] Obviously, such amount of monoclinic phase is insufficient for its detection by ATR technique. With increasing T_C up to 1000 °C, the contribution of monoclinic phase in XRD patterns rose up to $\approx 70\%$[15] and its presence is unambiguously detected by ATR spectra. However, for $T_C = 1100$ °C, the monoclinic phase content does not change practically, while the contribution of cubic phase increases slightly (Figure 2).

A high-energy spectral range of ATR spectrum shows the bands in the 1300–1400 cm^{-1}, 1500–1580 cm^{-1}, 1580–1680 cm^{-1}, and 3000–3700 cm^{-1} range. The latter one can be caused by stretching vibrations of OH-groups or water molecules.[19] The band at 1300–1400 cm^{-1} is explained by hydroxyl groups strongly bonded between themselves by hydrogen bonds and structured by hydroxyls of water (γ(OH)). The absorption at 1580–1680 cm^{-1} is attributed to deformation vibrations of adsorbed water, whereas the band at 1500–1580 cm^{-1} is assigned to the deformation vibrations of OH-groups bonded with the metal (δ(MOH)).[20] The intensities of the bands at 1580–1680 cm^{-1} and at 3000–3700 cm^{-1} decrease significantly with the increasing of T_C value in such a way that one can observe their vanishing in the S-set powders calcinated at $T_C \geq 900$ °C. Only weak bands of hydroxyl groups in the ranges of 1300–1400 and 1500–1580 cm^{-1} are still observed. However, the powder of R-set calcinated at 1100 °C showed significant contribution of the vibration bands at 1500–1580 and 3000–3700 cm^{-1} (Figure 2, curves 7,7').

Since the intensities of the absorption bands at 3000–3700 and 1580–1680 cm^{-1} change synchronously with the T_C rise and somewhat faster than the intensities of the other two bands (at 1300–1400 and 1500–1580 cm^{-1}), one can conclude that the band at 3000–3700 cm^{-1} can be also associated with adsorbed water.

It is worth to point out that water contained in the hydrogel evaporates at ≈ 200 °C (during drying), while the main amount of OH-groups is lost during the process of crystallization ($T_C = 400$–500 °C). However, Figure 2 shows the presence of OH-groups in our samples calcinated at higher temperatures. This, as well as the presence of adsorbed water, is obviously determined by the features of the nanocrystal surface.

3.3. Diffuse Reflectance Spectra

The UV-vis diffuse reflectance (DR) spectra of the powders calcinated at different temperatures and cooled with different rates are shown in **Figure 3**. These DR spectra contain the band
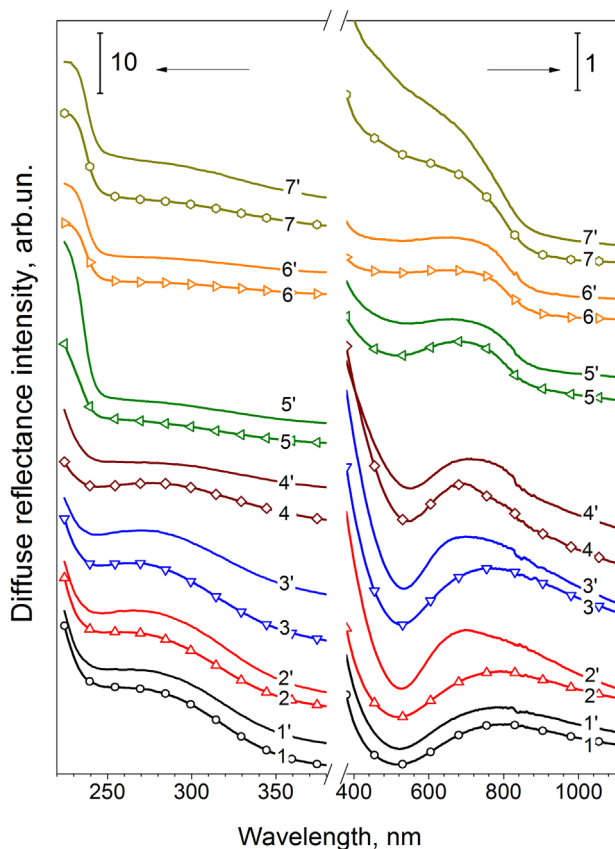
**ADVANCED
SCIENCE NEWS**

www.advancedsciencenews.com

pss
physica status solidi c

www.pss-c.com

Figure 3. Diffuse reflectance spectra of the powders calcinated at 500 (1, 1'), 600 (2, 2'), 700 (3, 3'), 800 (4, 4'), 900 (5, 5'), 1000 (6, 6'), and 1100 °C (7, 7') and submitted to a slow cooling (1–7) and quenching (1'–7').

The comparison of the spectra of the powders of the S- and R-sets calcinated at $T_C = 1100$ °C shows that the spectra of the "quenched" powders lead to higher signal intensities in the range of 500–600 nm. This effect can be explained by the appearance of an additional band, that can be connected with dispersed Cu clusters from which localized surface plasmon resonance can be observed in visible spectral range at about 570–585 nm.[24] Such clusters can be responsible for the appearance of the δ(MOH) and water-related vibration bands in ATR spectra due to OH and water absorption after quenching (Figure 2). Formation of such surface complexes can be seen from EPR spectra.

3.4. XRD and EPR Study of the Powders Calcinated at 1100 °C

Figure 4 represents the EPR spectra of the powders of S- and R-sets calcinated at 1100 °C. It is seen that slow cooling results in the appearance of a set of lines in a wide range (325–345 mT) of magnetic field (Figure 4, curve 1). The "quenched" powder demonstrates similar signal, but with lower intensity. Besides, a broad complex band at lower magnetic field appears (Figure 4, curve 2). Detailed study of the EPR spectra for the samples calcinated at lower T_C was reported in Ref. [12].

The analysis of both powders by XRD method showed that their structures are similar. Both monoclinic and tetragonal (cubic) phases can be seen (Figure 4, inset). The comparison of the contribution of m-ZrO$_2$ phase (peak at $2\Theta\sim28°$) and tetragonal (cubic) one ($2\Theta\sim30.2°$) shows that monoclinic-to-tetragonal ratio changes slightly. This means that the main difference between these powders is in the nature and/or

(peaked at ≈275 nm) near the band edge of ZrO$_2$. The T_C rise in the range of 500–700 °C leads to a slight increase of its intensity while for $T_C = 800$–1100 °C, the intensity of this band decreases essentially in both groups of samples. The decrease of the intensity of the 275-nm band is accompanied by the anti-correlation with the increasing of the monoclinic phase content (Figure 1 and 2). This phase is known to contain lower number of oxygen vacancies than tetragonal phase stabilized with Y- or Cu impurities.[12,21] It allows assigning the band at ≈275 nm observed in our samples to oxygen vacancies.

In addition to the band at ≈275 nm, another band in the range of 600–900 nm is observed. Its intensity increases with T_C rising up to 800 °C and its peak position shifts to shorter wavelengths. For the higher cooling rate, the more pronounced contribution of this band in the spectra can be observed for $T_C = 600$–800 °C (Figure 3).

This band is usually attributed to d–d transitions of Cu^{2+} ions in an octahedral or tetragonal distorted octahedral surrounding[21,22] and associated with dispersed CuO on the surface of the nanocrystals[20] or with Cu$_{Zr}$ substitutional atoms located near the surface of the nanocrystals.[9,21] The observed high-energy shift of this Cu-related band with T_C in both cases was explained by an increase of octahedral distortion.[21,23] As shown by Figure 3, the edge of the fundamental absorption of crystalline CuO is observed for powders calcinated for $T_C = 900$–1000 °C.
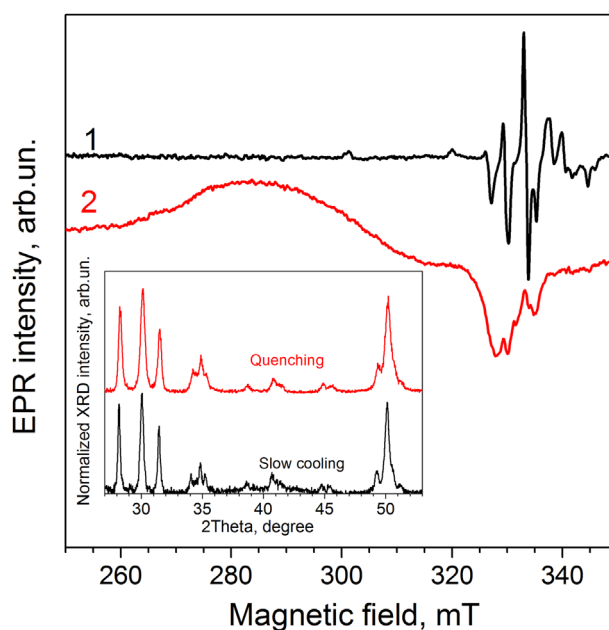

Figure 4. EPR spectra of the powders calcinated at 1110 °C upon slow cooling (1) and quenching (2). Corresponding XRD data are shown in the inset.

ADVANCED
SCIENCE NEWS

www.advancedsciencenews.com

physica
pss status solidi c

www.pss-c.com

amount of the surface entities because coherent domain size, estimated from XRD data, is similar for both powders.

Comparison of Figure 2 and 4 shows that quenching results in the simultaneous appearance of broad EPR signal and infrared absorption bands related to OH-groups and H_2O molecules contrary to slow cooling. Thus, such a broad EPR signal can be ascribed to the surface complexes containing copper ions linked with water molecules and/or OH-groups. Similar results were reported in Refs. [12,25].

It is worth to point out that the set of narrow EPR lines in a wide range of magnetic fields (and therefore the absence of spin-Hamiltonian parameters distribution) indicates that the paramagnetic centers responsible for this spectrum are in regular positions with stable surrounding. Besides, the presence of characteristic hyperfine lines allows reasonable assuming that this spectrum (or at least its main part) is caused by substitutional Cu^{2+} ions (Cu_{Zr}^{2+}). Since this signal intensity correlates with the contribution of m-ZrO_2 phase,[12] one can assume that this signal is caused by Cu_{Zr}^{2+} ions in the monoclinic structure. The absence of signal of Cu_{Zr}^{2+} ions in the tetragonal structure can be related, for example, with rapid spin relaxation processes or another Cu charge state.

The analysis of the results described above shows that effect of calcination temperature and cooling rate is determined by three processes: i) the decomposition of surface Cu-OH (or Cu-H_2O) complexes revealed in EPR spectra and their transformation to CuO and Cu; ii) Cu in-diffusion from Cu-related surface entities that dominates at $T_C \leq 800\,°C$ and is accompanied by the increase of oxygen-vacancy related band (at 275-nm) in diffuse reflectance spectra; iii) Cu outward migration from the bulk to the grain surface that dominates at $T_C > 800\,°C$, stimulates Y out-diffusion, results in t-m ZrO_2 transformation and decrease of EPR signal from substitutional Cu. The increase of calcination temperature stimulates the enrichment of grain surface with CuO or pure Cu whatever the cooling rate. However, the higher the cooling rate, the higher the Cu (CuO) content at grain surface can be seen. This phenomenon is determined by the balance between the processes of "in-diffusion" and "out-diffusion" of copper ions. The calcination temperature increase shifts this balance towards Cu out-diffusion. In this regard, a higher cooling rate (quenching) allows "freezing" the state corresponding to higher T_C and, thus, the higher surface Cu content. This statement was confirmed by the properties of the powder calcinated at 1100 °C. It is obvious that the high amount of surface CuO or Cu clusters in this powder after its quenching is responsible for water adsorption (Figure 2) and appearance of broad EPR signal (Figure 4).

It is worth to point that the behavior of copper ions with respect to the cooling rate can affect also the catalytic properties of the powders. The catalytic activity of these latter is under investigation and it is a subject of future publications.

4. Conclusions

The effect of calcination temperature and cooling rate on copper localization in ZrO_2 composites doped with Y and Cu was studied by ATR, diffuse reflectance, XRD, EPR, and TEM techniques. It was observed that $T_C = 800\,°C$ is a critical temperature that influences the dominating type of diffusion process. Below this T_C value, the Cu diffusion inside ZrO_2 grains prevails and stabilizes the tetragonal phase. For higher T_C values, the outward migration of Cu and then, Y ions results in the destabilization of the tetragonal phase. The cooling rate allows tuning the nature and distribution of Cu-related substances located at grain surfaces.

Conflict of Interest

The authors declare no conflict of interest.

[1] K. Tanabe, *Mater. Chem. Phys.* **1985**, *13*, 347.
[2] P. Bansal, G. R. Chaudhary, S. K. Mehta, *Chem. Eng. J.* **2015**, *280*, 475.
[3] T. Tsoncheva, I. Genova, M. Dimitrov, E. Sarcadi-Priboczki, A. M. Venezia, D. Kovacheva, N. Scotti, V. dal Santo, *Appl. Catal. B* **2015**, *165*, 599.
[4] L. C. Wang, Q. Liu, M. Chen, Y. M. Liu, Y. Cao, H. Y. He, K. N. Fan, *J. Phys. Chem. C* **2007**, *111*, 16549.
[5] M. D. Rhodes, K. A. Pokrovski, A. T. Bell, *J. Catal.* **2005**, *233*, 210.
[6] M. D. Rhodes, A. T. Bell, *J. Catal.* **2005**, *233*, 198.
[7] Z. Y. Ma, C. Yang, W. Wei, W. H. Li, Y. H. Sun, *J. Mol. Catal. A* **2005**, *231*, 75.
[8] J. Sun, P. A. Sermon, *Catal. Lett.* **1994**, *29*, 361.
[9] K. Samson, M. Śliwa, R. P. Socha, K. Góra-Marek, D. Mucha, D. Rutkowska-Zbik, J. F. Paul, M. Ruggiero-Mikołajczyk, R. Grabowski, J. Słoczyński, *ACS Catal.* **2014**, *4*, 3730.
[10] F. F. Qu, W. Chu, L. M. Shi, M. H. Chen, J. Y. Hu, *Chin. Chem. Lett.* **2007**, *18*, 993.
[11] S. N. Basahel, M. Mokhtar, E. H. Alsharaeh, T. T. Ali, H. A. Mahmoud, K. Narasimharao, *Catalysts* **2016**, *6*, 57.
[12] N. Korsunska, M. Baran, I. Vorona, V. Nosenko, S. Lavoryk, X. Portier, L. Khomenkova, *Nanoscale Res. Lett.* **2017**, *12*, 157.
[13] Y. Zhang, L. Hu, H. K. Li, J. Chen, *J. Am. Ceram. Soc.* **2008**, *91*, 1332.
[14] N. Korsunska, M. Baran, Yu. Polishchuk, O. Kolomys, T. Stara, M. Kharchenko, O. Gorban, V. Strelchuk, Ye. Venger, V. Kladko, L. Khomenkova, *ECS J. Solid State Sci. Technol.* **2015**, *4*, N103.
[15] N. Korsunska, Yu. Polishchuk, V. Kladko, X. Portier, L. Khomenkova, *Mater. Res. Express* **2017**, *4*, 035024.
[16] N. Korsunska, M. Baran, A. Zhuk, Yu. Polishchuk, T. Stara, V. Kladko, Yu. Bacherikov, Ye. Venger, T. Konstantinova, L. Khomenkova, *Mater. Res. Express* **2014**, *1*, 045011.
[17] N. Korsunska, A. Zhuk, V. Papusha, O. Kolomys, Y. Polishchuk, Y. Bacherikov, V. Strelchuk, V. Kladko, T. Konstantinova, T. Kryshtab, L. Khomenkova, in *Materials Characterization* (Eds: R. Pérez Campos,

A. Contreras Cuevas, R. Esparza Muñoz), Springer International Publishing, Switzerland **2015**, Ch. 7.

[18] D. W. Liu, C. H. Perry, R. P. Ingel, *J. Appl. Phys.* **1988**, *64*, 1413.

[19] T. López, M. Alvarez, R. Gómez, D. H. Aguilar, P. Quintana, *J. Sol-Gel. Sci. Technol*. **2005**, *33*, 93.

[20] B. O. Cho, S. X. Lao, J. P. Chang, *J. Appl. Phys.* **2003**, *93*, 9345.

[21] V. P. Pakharukova, E. M. Moroz, V. V. Kriventsov, T. V. Larina, A. I. Boronin, L. Yu. Dolgikh, P. E. Strizhak, *J. Phys. Chem. C* **2009**, *113*, 21368.

[22] J. P. Goff, W. Hayes, S. Hull, M. T. Hutchings, K. N. Clausen, *Phys. Rev. B* **1999**, *59*, 14202.

[23] I. P. Bykov, A. B. Brik, V. V. Bevz, T. E. Konstantinova, I. A. Yashchishin, *Nanosistemi, Nanomateriali, Nanotehnologii* **2009**, *7*, 543.

[24] C. C. Crane, F. Wang, J. Li, J. Tao, Y. Zhu, J. Chen, *J. Phys. Chem. C* **2017**, *121*, 5684.

[25] O. Gorban, S. Gorban, O. Zarechnaya, M. Kharchenko, T. Konstantinova, in *Nanophysics, Nanophotonics, Surface Studies, and Applications* (Eds: O. Fesenko, L. Yatsenko), Springer Proceedings in Physics, vol. 183, Springer International Publishing, Switzerland **2016**, Ch. 44.